Percolation, Localization, and Superconductivity

Edited by

Allen M. Goldman

School of Physics and Astronomy
University of Minnesota
Minneapolis, Minnesota

and

Stuart A. Wolf

Metal Physics Branch
Naval Research Laboratory
Washington,D.C.

Plenum Press
New York and London
Published in cooperation with NATO Scientific Affairs Division

MICROFABRICATION TECHNIQUES FOR STUDIES OF PERCOLATION, LOCALIZATION, AND SUPERCONDUCTIVITY, AND RECENT EXPERIMENTAL RESULTS

Daniel E. Prober

Applied Physics
Yale University
New Haven, CT 06520

INTRODUCTION

In the past four years studies of localization and percolation in lower-dimensional systems have been conducted in a number of laboratories. These studies have advanced in a fundamental way our understanding of electron transport in dirty and inhomogeneous systems. The production of the experimental systems has relied directly on advanced microfabrication techniques. It is the purpose of this chapter to review these techniques and also selected experimental results for systems whose production exemplifies these microfabrication techniques.

The model systems which we shall discuss include metal line structures as small as 200 Å, produced with step-edge techniques. These have been used in studies of one-dimensional (1D) conduction effects. Experiments on MOSFETs (Metal-Oxide-Semiconductor-Field-Effect Transistors) have allowed study of the 2D electron gas, and with further lithographic patterning, nearly-1D MOSFETs have been produced. Finally, arrays of superconducting tunnel junctions have served as model 2D superconducting systems.

The examples of model systems listed above demonstrate the range of experiments which are now accessible to researchers at both universities and at major research laboratories. The studies have involved both engineering technologists and basic scientists, and their success demonstrates the viability of the subfield of microstructure science. As we shall see, the techniques are particularly well suited for studies of electron localization, percolation, and superconductivity, because intrinsic length scales for these phenomena can be in the range 1000 to 10,000 Å.

In this chapter we outline the basic principles, current capabilities and limits, and future possibilities of modern microfabrication techniques. There have been numerous reviews of specific microfabrication techniques, intended for an audience of scientific users[1,2] or engineering practitioners of the art.[3-5] The reader may consult these reviews and the references therein for specifics on implementing the varied techniques we shall discuss.

LITHOGRAPHY PROCESSES

Resist Processes and Resolution Limits

In current lithographic practice, incident radiation (photons, electrons, or ions) is used to "expose" areas of a thin polymer layer (the "resist"). In the exposed areas the resist has a modified removal rate in a suitable developer. For a positive resist the exposed areas develop faster. The exposure process involves the breaking of chemical bonds, polymer crosslinking, or initiation of chemical reactions. With electron, ion, and x-ray exposure, low-energy (<100 eV) electrons are ultimately produced. These "secondary" electrons have a large cross section for interaction with the resist. Thus, the ultimate limit on resolution is set by the path-length of these low-energy electrons, typically <100 Å.[4] The exposure resolution of modern photoresists can be as good as the resolution of the exposure system itself. For diffraction-limited exposure systems the resist resolution is thus comparable to the wavelength, ~4000 Å.

A simple optical exposure system based on a high quality optical microscope[6] is diagrammed in Fig. 1. Here, a mask of the desired pattern is placed in the microscope field stop. A demagnified image of this pattern is projected onto the photoresist. (In Fig. 1 the light is shown being projected <u>through</u> a transparent substrate. This gives edge profiles[6] which are more favorable for use with the lift-off process, discussed below. This through-the-substrate exposure is convenient, but not essential.) With this system, a pattern resolution of 0.2 μm (2000 Å) can be achieved for simple line patterns. The field of view is small, <0.2 mm, for lenses with this resolution.

After the exposed resist is developed, the pattern can be transferred in one of two ways: 1. subtractive etching, in which the photoresist protects the underlying film or substrate, and 2. additive deposition, in which a film is deposited on the resist and on areas not covered by the resist. For this second case, the resist is then dissolved, and the film on top of the resist is removed (see Fig. 1). This is the lift-off process. It is widely used for research patterning of submicron structures. (Note: 1 micron ≡ 1 μm = 10,000 Å) Photoresist edge profiles which are undercut, as shown in Fig. 2, ensure clean liftoff.

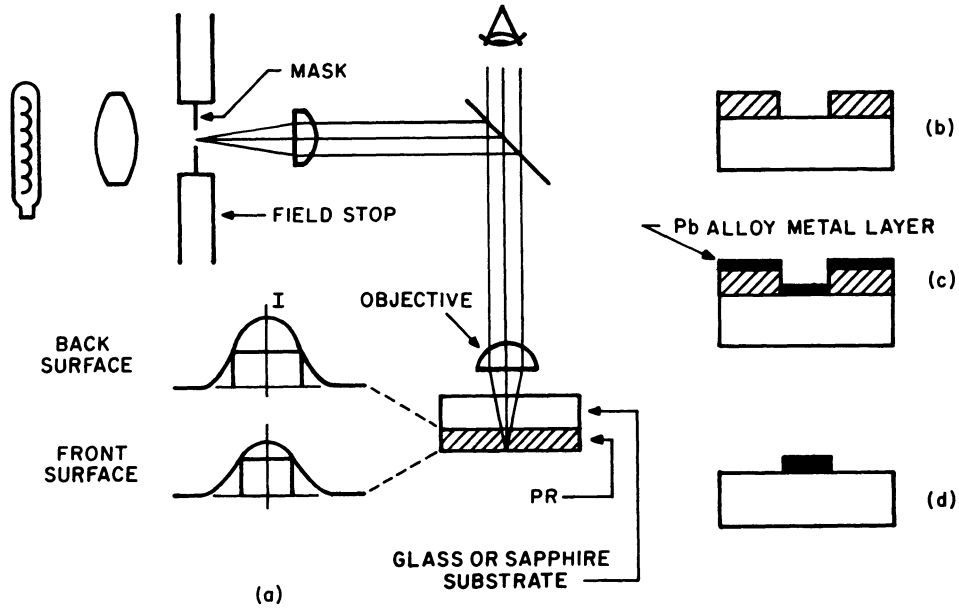

Fig. 1. Schematic of the projection microscope and lift-off procedure. (a) Projection exposure of the photoresist (PR) in a reflected-light microscope. Schematic intensity (I) of exposing radiation vs. position at two heights in PR is also shown; (b) after development; (c) following metallization; and (d) results of lift-off.

Pattern transfer by subtractive etching is required when a photoresist lift-off mask cannot withstand the deposition conditions. For example, temperature limits of ∿150° to 200°C apply for conventional resists, although some high temperature lift-off processes have been developed.[7] The selection of etching or lift-off may be determined by other considerations. Lift-off is well suited for producing a fine metal line, for example, but not for producing a small gap between two electrodes.

In the past 3 years it has been recognized that many of the resolution limits which were once thought to be intrinsic are not fundamental to the exposure process, but rather resulted from using single-layer resists with properties chosen to meet conflicting requirements. The resist layer must be thick to smoothly cover topography resulting from previous processes so as to avoid defects. (This consideration is of central importance in semiconductor device production, where many mask levels are required.) However, thick layers allow spreading of the incident radiation (due to scattering or diffraction), sidewards development (while development proceeds through the resist thickness), and standing-wave effects in the resist (for optical exposure).

The recent perfection of a number of multilayer resists[8] has resolved most of the conflicting requirements for the resist. Multilayer resists consist of a thin top layer, sometimes with an intermediate layer, and a thicker bottom layer for topography smoothing. (A two layer resist is shown in Fig. 2b.) The characteristics of each layer can be optimized independently. The top layer is optimized for resolution, the bottom layer for coverage. Using a multilayer resist, a standard scanning electron microscope can be used to expose 250-Å linewidth patterns.[9] In addition to the finite electron beam size, ∿100 Å, the factors determining resist resolution are the secondary electron pathlength, and the size of the coiled up polymer in the polymethylmethacrylate resist (PMMA). Limits on resist resolution are summarized in Table I.

The utility of multilayer photoresists is also seen in semiconductor device production. Hewlett-Packard has achieved a significant increase in yield for their 450,000 transistor chip when a multilayer resist process was introduced.[10] This chip serves as the processor in their 32-bit Model 9000 computer. The chip uses a lithographically aggressive design, with 1.5 μm lines and 1 μm spaces.

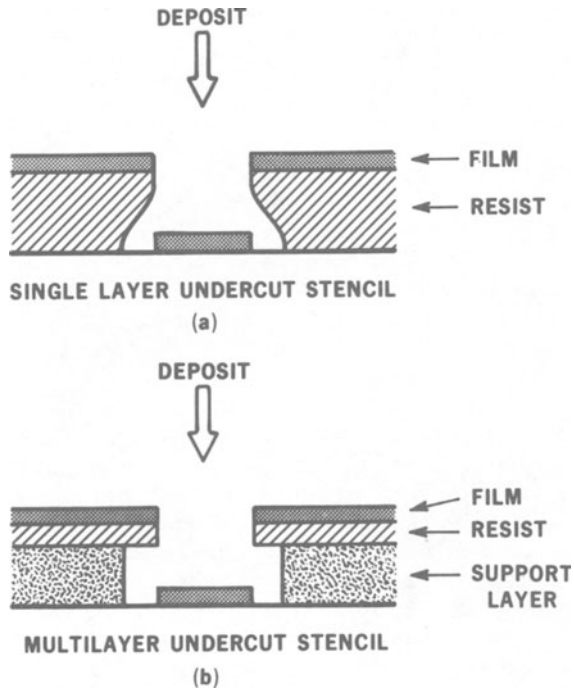

Fig. 2. Application of undercut resist profiles to lift-off.

Table I. Resolution and Other Patterning Limits

Mechanism	Resulting Limit
Pathlength of low-energy electron	∿100 Å
Polymer structure	Not established; <100 Å
Exposure statistics	<100 Å (PMMA)
Diffraction (x-ray) or scattering in resist (electron, ion exposure)	<100 Å for thin resist layer
Electron backscattering from thick substrate	Loss of contrast
Processing temperature	<150°C, most resists

Exposure Systems

Exposure instruments for use in a research environment have been developed by a number of researchers.[2,6,9] For optical exposure, it has proven sufficient to use a high quality optical microscope.[6] A resolution of 0.2 to 0.5 μm can be achieved with care. This resolution is set by the diffraction-limited optics. Alignment, at least to 1 μm accuracy, can be accomplished with red light, which does not expose the resist. The field of view of these instruments is limited (∿0.2 mm for a typical 100X lens). Commercial optical projection systems typically achieve 1 μm resolution over a 1 cm field of view, and can align to 0.25 μm.

For electron beam exposure, a standard scanning electron microscope (SEM) can be used. A resolution of 250 Å has been achieved,[9] though careful control of the exposure dose is essential. Alignment is not trivial, since the entire substrate surface is coated with resist. Even smaller linewidths have been achieved with a scanning transmission electron microscope (STEM), which can readily achieve a beam diameter of 20 Å. On solid substrates, 100 Å lines have been produced.[11] Since the sample is inserted into the magnetic lens, its dimensions are limited to <3 mm.

Electron beam exposure may be controlled with either a flying-spot scanner,[12] or with a computer which turns the beam on or off and simultaneously drives (or is synchronized with) the X and Y

beam sweeps. It is most convenient to use a beam blanker to turn the beam on and off. Simple schemes which instead "dump" the beam in an unused area of the substrate may be acceptable, but only for slow writing (due to deflection-coil response).

The resist employed in nearly all research uses of electron beam lithography is PMMA. This resist has the best resolution known. PMMA also requires a relatively large exposure dose, so that intrinsic statistical fluctuations of the exposing beam are relatively small, even for exposed areas as small as 100 Å x 100 Å.[1] Conversely, PMMA is generally considered to be too slow (insensitive) for commercial applications.

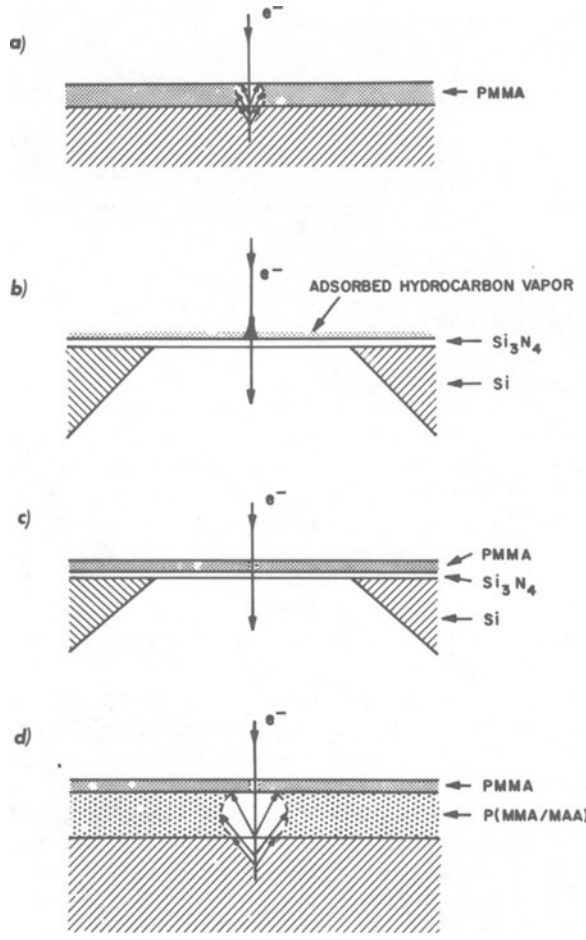

Fig. 3. Electron-beam exposure showing scattering and methods to reduce scattering. (a) thick resist; (b) contamination-resist lithography on a membrane; (c) polymer resist on a membrane; (d) high-resolution two-layer resist.

The size of the coiled-up PMMA polymer is <100 Å. Use of a resist with a smaller "grain size" might lead to even better resolution than is achieved with PMMA. IBM researchers have developed a contamination writing technique in which the electron beam converts residual organic contamination on the substrate surface into a hard carbonaceous material. This contamination resist can be used as an etch mask for Ar-ion etching. Au-Pd lines 80 Å wide have been produced with exposure in a STEM. Very careful control of the exposure intensity is required to achieve this smallest dimension. Contamination resist techniques are discussed in detail in a separate chapter.[13]

Fig. 3 shows the various configurations for electron beam exposure. Both lateral beam spreading and backscatter from the substrate are observed with a thick resist (Fig. 3a). Use of a multilayer resist, Fig. 3d, can largely eliminate these problems. Use of a thin membrane substrate, as shown in Fig. 3b and 3c, eliminates electron backscattering, and also allows inspection of the final structure in STEM or TEM instruments, which have better resolution (typically <10 to 20 Å) than usual SEMs (resolution ∿100 Å).

Table II. Pattern Resolution Achieved

Exposure Method	Exposure Process (and Reference)	Resolution[a]	Field of View[a]
Optical	Microscope projection[6]	2000 Å	200 μm
	Commercial projection system[5]	1 μm	1 cm
Electron beam	SEM, PMMA[9]	250 Å	100 μm[b]
	STEM, PMMA[11]	100 Å	30 μm[b]
	JEOL lithography system (25 kV), PMMA	≤200 Å[c]	100 μm[c]
	STEM, contamination resist[13]	80 Å	-
X-ray	C_K x-ray source, PMMA[15]	175 Å	1 cm

[a] Figures given are intended primarily as a general guide, but reflect actual values where available.

[b] R. E. Howard, private communication.

[c] G. J. Dolan, private communication.

Membrane substrates are particularly well suited to experiments on thin metal films, but still do not have the general applicability of the approach of Fig. 3d.

X-ray and ion-beam exposure of resist have not been widely used for laboratory studies, but are under active investigation for semiconductor device production. X-ray exposure is currently done only as a 1-to-1 contact printing process, so that mask fabrication must be done by some other high resolution process. Flanders[14] has developed a very useful exposure system and polyimide membrane mask system. A printing resolution of ∿175 Å is achieved.[15] Ion beam lithography has to date been limited in resolution by the exposing beam size (∿400 Å), but should have an intrinsic resolution of ∿100 Å. The performance characteristics of the various exposure systems is given in Table II.

Etching and Deposition

Film patterning by etching employs either liquid or ion/plasma etchants. Liquid etching in general has the greatest material selectivity, but has the disadvantage that the liquid will also etch under the mask. (One exception is the use of anisotropic liquid etchants which etch different crystal planes of a single crystal at different rates. Such etchants for silicon are well studied.[16a]) Anodization is a liquid process which can convert many metals into their insulators. It has good dimensional resolution, and is particularly useful for patterning refractory superconductor films.[16b]

Ion or plasma etching[17] can be very directional. Material selectivity can be fair, or good to excellent, depending on whether an inert gas (e.g., Ar) or a chemically reactive gas is used. For Ar ion etching mechanical momentum transfer causes the etching. In reactive ion etching the gas forms reaction products with the material to be etched. These products are usually gases, which rapidly leave the surface and do not redeposit elsewhere. An example of such a case is the simplified reaction of CF_4 etching Si, where SiF_4, a gas, can in the end be formed. There is some amount of mechanical bombardment in all ion etching processes, so that the selectivity is rarely as good as with liquid etchants. It is only with ion etching, however, that one can etch deep slot structures or steps in polycrystalline films.

Methods of patterning which employ ion etching can achieve very high resolution, sometimes limited only by the grain size of the film to be etched. For this reason and for reasons of temperature stability, fine-grain alloy films are often desired. Examples include Au-Pd and W-Re, both used to form narrow (∿200 Å) wires. It is however possible to produce continuous and uniform films of some elements. Aluminum is an example. Cleaning the substrate by ion

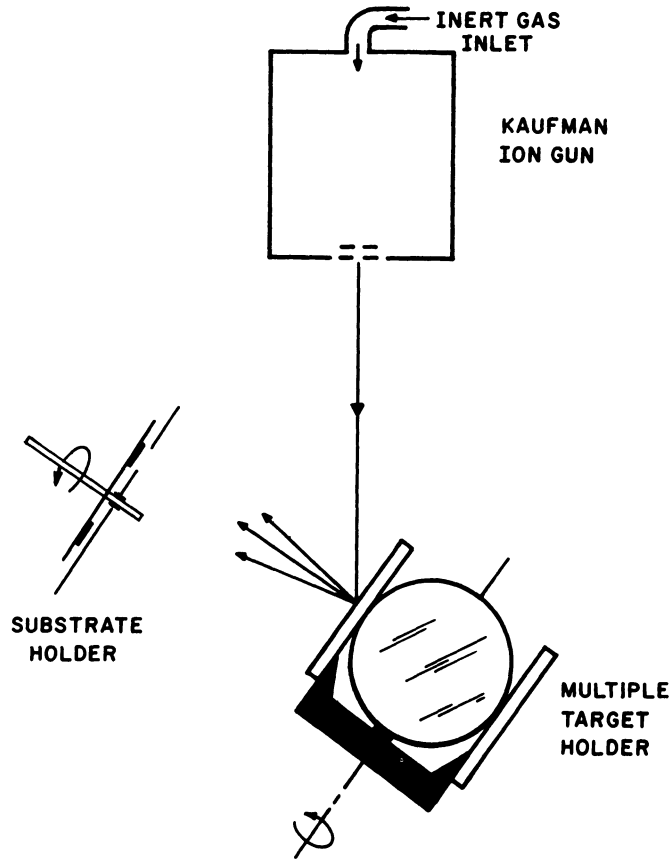

Fig. 4. Schematic of ion beam sputter deposition system, comprising a 2.5 cm Kaufman ion source, multiple target holder accommodating four 4 in. targets, and substrate holder (From Ref. 18).

etching immediately before film deposition can be critical to achieving uniform coverage and good adhesion. Such cleaning must be done "in-situ," that is, without breaking vacuum.

Sputtering can also be employed in deposition processes. Fig. 4 shows an ion beam sputter deposition system developed at Yale, which is used for depositing high quality films of refractory superconductors.[18] This sputtering system allows deposition of layers of different materials in rapid succession, to avoid interface contamination. This type of system is particularly useful in producing artificial tunneling barriers on refractory supercon-

ductors.[16b,19] In addition, certain materials, such as Ta, can be "coaxed" into growing in the desired crystal structure by deposition onto an appropriate underlayer film.[18] In general, for sputtering the directionality of deposition is not as good as with thermal evaporation. Such directional deposition is required for some of the three dimensional methods described below.

Three-Dimensional Techniques

In previous sections we have described various types of direct lithography - that is, techniques which provide a direct replica of the exposed pattern. These direct techniques are not the only, nor even the simplest, methods for producing structures on a size scale <1000 Å. A variety of innovative three-dimensional (3D) techniques which utilize edges and shadowing have been developed to fold over a height dimension into a feature dimension. These techniques can be very effective when a high aspect ratio, of height to width, is required, and they are well suited to smaller research laboratories.

Two types of edge-defined processes[20] are shown in Fig. 5.

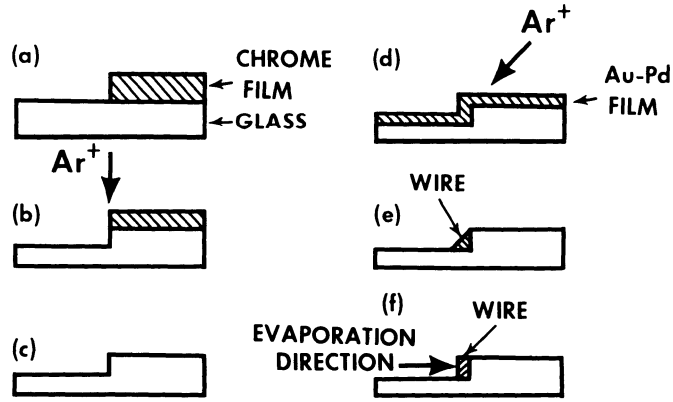

Fig. 5. Wire fabrication procedures. The substrate is shown in side view: a. Half the substrate is coated with a thin chrome film. b. The substrate is ion etched to produce a square step. c. The chrome film is removed with a chemical etch. d. The substrate is coated with the metal film and ion etched at an angle until, e. a triangular wire is formed along the step edge. (Alternate process) f. The metal film is evaporated parallel to the substrate to coat only the step edge. (From Ref. 20)

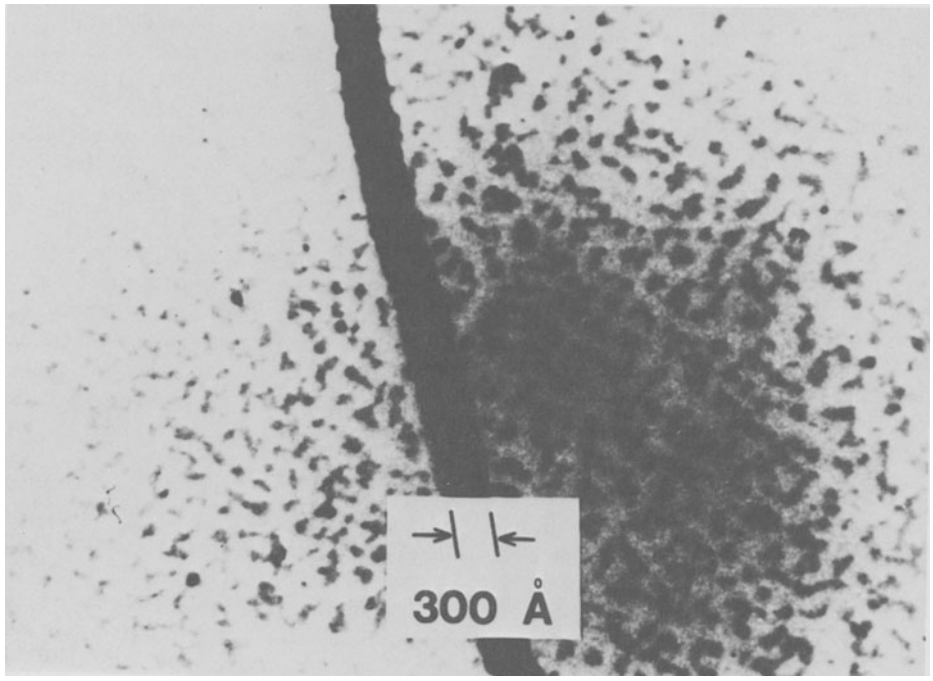

Fig. 6. Rectangular Ni wire, with 300 Å linewidth, formed on the edge of a step in SiO_2; transmission electron micrograph. (From Flanders and White, Ref. 14)

The first process consists of steps a thru e, and is used to form a triangular wire. The substrate step protects the metal in its "shadow" from ion etching (step d). A relatively soft material such as Au-Pd, which etches faster than glass, can be patterned in this fashion. For the angles shown, the step height sets the linewidth. Since height dimensions can be controlled to <50 Å by setting the etching time (step b), wires smaller than 200 Å can be formed. The factors which in practice limit wire dimensions are the raggedness of the photoresist lift-off mask (used for patterning the chrome etch mask), the grain size of the chrome etch mask, and finally the grain size of the Au-Pd metal film. As can be seen in Fig. 5, this process is self aligning; as a result, it has a high yield. Also, although lift-off photolithography is used, there is no diffraction limit *per se*, since only edges are employed. These edges are formed with high contrast processes. The triangular wires produced with this procedure were used in extensive studies of electron localization, described later in this chapter.

The second process for forming a narrow wire consists of steps

a thru c and f in Fig. 5. Here the wire is evaporated directly on the step edge. The film thickness determines one of the wire dimensions, the step height the other. With this second process there is no requirement that the metal film etch faster than the glass. Wires as small as 200 Å have also been produced with this process. An example of such a wire, formed on a membrane substrate, is shown in Fig. 6. The excellent uniformity and edge definition show the power of this technique. Only optical lithography was used to define the lift-off mask.

More complex structures can also be patterned with step edges. It is possible to produce in this way very small superconducting microbridges, the thin film analogue of a point contact structure, in which all dimensions are <500 Å.[21] Two steps are used, with an angle-shadowed mask required for the etch mask of the second step. One step height sets the bridge length, the other the bridge width. Improved electrical performance results from the small size.

In analogy to the above approach, it is possible to make very short SNS microbridges, by depositing the superconducting (S) electrodes and the normal (N) metal bridge from different angles. High-T_c SNS microbridges have been formed for the first time with this technique.[22] The superconducting film, Nb_3Sn or Nb_3Ge, must be deposited at ∿800°C. This is possible because no resists are used for device patterning. The substrate (silicon on sapphire) may thus be heated during deposition. Linear arrays of SNS microbridges have been patterned with this technique. See Fig. 14 for a diagram.

The three dimensional techniques discussed above all utilize substrate patterning. Three dimensional resist structures can also be produced with multilayer resists. A useful and very elegant approach has been developed by Dolan for self- aligned fabrication of metal-oxide-metal superconducting tunnel junctions.[23] This approach is shown in Fig. 7. A tunnel junction is formed by depositing the first metal film, oxidizing it, and from the opposite direction (2) depositing the second film. The tunnel junction is thus formed without exposure to atmosphere (for lithography) or sputter cleaning between the two evaporations. As a result, one can produce small, high-current-density tunnel junctions much more easily than with conventional Josephson junction processes. Junctions produced with the Dolan process have been used in studies of macroscopic quantum tunneling[24] and as low-noise microwave mixers.[25] Arrays of such junctions are also useful for studying 2D superconducting phase transitions.

In this section we have discussed the capabilities of various lithographic techniques, and shown some examples of the results achieved. In the next section we present the major applications of microlithography in the areas of localization and superconductivity related to theoretical issues discussed in the rest of this volume.

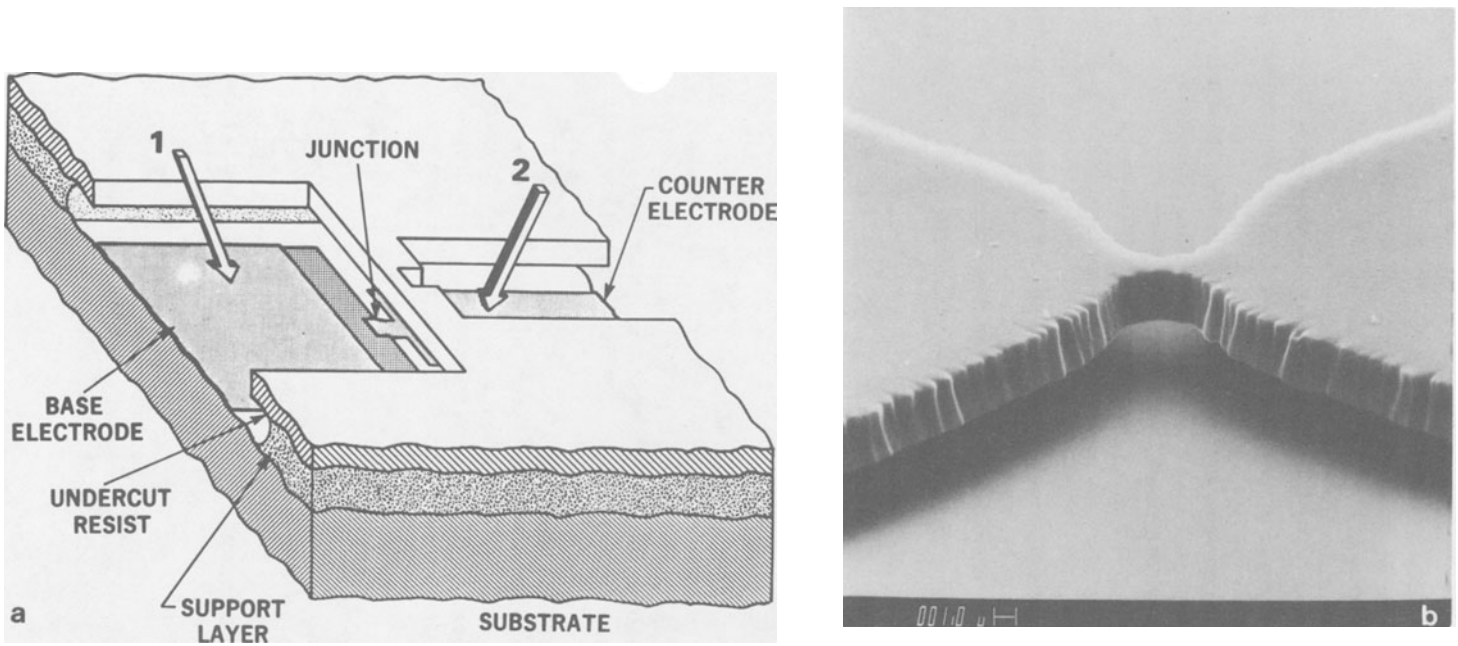

Fig. 7. Self-aligned tunnel junction fabrication, patterned with a multilayer resist stencil. The base electrode is oxidized prior to deposition of the counter electrode. a. Schematic outline; b. SEM of photoresist structure, by P. Santhanam (unpublished) for work of Ref. 25b. View is from a different orientation than Fig. a. Resist thickness is 2 μm for both the suspended layer and the support layer (not visible in Fig. b). (Fig. 7a from Ref. 1.)

SCIENTIFIC STUDIES: ELECTRON LOCALIZATION AND INTERACTION EFFECTS

In 1977, D. Thouless made a striking prediction[28] - that at T = 0, all wires should behave as insulators, due to electron localization effects. The only requirement is that the wires be long enough. This length requirement translates into a resistance requirement, that the high-temperature (e.g., 10K) resistance of the wire be greater than $\sim$10 kΩ. Since this prediction, theoretical understanding of electron localization has advanced at a remarkable rate. Two excellent theoretical reviews from different points of view are given in this volume.[26]

In this section we review the requirements on experimental systems with regard to dimensionality and size, and discuss the experimental approaches which have been developed for producing effectively one dimensional (1D) systems. We also discuss two recent sets of experiments, on metal wires and films, and on narrow MOSFETs. We concentrate largely on 1D studies, since these require special microfabrication techniques. Studies on 2D systems require the production of very thin, continuous films or granular films. These issues are discussed elsewhere in this volume, in the chapters by Beasley, by Deutscher, and by Laibowitz.

General Considerations: Dimensional Requirements and Inelastic Times

Experiments to probe localization and electron-electron interaction effects have utilized studies of resistance, magnetoresistance, Hall effect, thermoelectric effect, and tunneling density of states. In all cases the theoretical prediction depends on sample dimensionality, and it is this aspect which can be controlled with microfabrication techniques.

At low temperatures, an experimental sample may act as a system of reduced dimensionality even though it is large compared to atomic dimensions. For localization, the relevant length scale is the Thouless length, which for finite temperatures is given as

$$L_{Thouless} = \ell_{in} = (D\tau_{in})^{1/2} \qquad (1)$$

with ℓ_{in} the inelastic diffusion length, D the diffusion constant ($= v_F^2\tau/3$ in 3D systems; τ is the elastic scattering time), and τ_{in} is the time between inelastic collisions. Weak (small) localization effects are expected when ℓ_{in} is less than the localization length.[26a] This is the usual experimental situation.

We list in Table III the essential temperature dependence of the inelastic scattering rate, τ_{in}^{-1}, for electron-phonon and electron-

Table III. Temperature Dependence of Inelastic Scattering Rates

Mechanism	System	Dimension	τ_{in}^{-1}	Ref.
Electron-phonon (system dimension set by λ_{phonon})	Clean	3D	T^3	28
		2D	T^2	28
		1D	T	28
	Dirty ($q_{phonon}\ell<1$)	3D	T^4	28,27a*
		3D	T^2	27b*
		2D	T^3	28
		1D	T^2	28
Electron-electron (system dimension set by L_{int})	Clean	3D	T^2	27c
		2D	$T^2 \ln T$	27c
		1D	T	27c
	Dirty ($\tau<\frac{\hbar}{kT}$)	3D	$T^{3/2}$	27d
		2D	$T \ln(T_1/T)\sim T$**	27d
		2D	$T \ln(\text{const})\sim T$	27e
		2D	T	27f
		1D	$T^{1/2}$	27d

*See Ref. 27b for a discussion of these differences.

**Since $T_1 >> T$, the essential dependence on temperature is just $\sim T$.

electron scattering in both clean and dirty systems. "Clean" and "dirty" are defined in the table. Mechanisms are discussed in the references.[26-28]

For electron-electron interaction effects the length scale which determines system dimensionality is the quantum diffusion length

$$L_{int} = \left(\frac{D\hbar}{kT}\right)^{1/2}. \tag{2}$$

L_{int} thus depends on temperature and on the elastic scattering time (through D). The mean free path is given as $\ell = v_F\tau$.

The length scale ℓ_{in} or L_{int} usually enters the theoretical prediction for quantum corrections to transport properties at low temperatures. For example, for 1D localization effects the resistance is increased above the Boltzmann (elastic) term by[28]

$$\frac{\Delta R^{1D}}{R} \sim \frac{\ell_{in}}{L_{36.5k\Omega}}. \tag{3}$$

$L_{36.5k}$ is the length of wire which at high temperature (~10K) has $R = 36.5\ k\Omega$. A similar formula holds for 1D interaction effects, but with L_{int} instead of ℓ_{in}. Here and in nearly all other experiments, the temperature dependence of the predicted effect is an essential feature, as τ_{in} depends on temperature, as does L_{int}.

It appears that a system may be of a certain dimensionality for determining the inelastic scattering process, yet of a different dimensionality with respect to localization. Thus, the scattering mechanism for a narrow wire need not be a 1D mechanism, even if 1D localization theory is applicable. Also, the total scattering rate is the sum of the rates due to all inelastic processes which contribute significantly. Thus, τ_{in}^{-1} need not have the simple temperature dependence T^p, with p an integer.

Experiments on 1D Metal Wires - Early Work

The theoretical predictions by Thouless of 1D localization effects inspired a number of experiments. The earliest of these 1D localization studies were at Yale.[29] In these studies, triangular wires of Au-Pd were produced with the novel step edge technique (Fig. 5a-e) discussed earlier. These and subsequent experiments by Giordano[30] showed a resistance which increased with decreasing temperature. The form of the measured increase was

$$\frac{\Delta R}{R} \sim \frac{\rho T^{-1/2}}{A}. \tag{4}$$

A is the cross sectional area, ρ the resistivity. The A^{-1} dependence is as expected; it is implicit in Eq. 3. The experimental $T^{-1/2}$ dependence, however, is weaker than predicted by Eq. 3 for the expected inelastic scattering mechanisms, unless $\tau_{in}^{-1} \sim T$. In addi-

tion, the dependence on ρ is not that expected from Eq. 3, which predicts that $\Delta R/R \sim \rho^{1/2}$ for τ_{in} independent of ρ and $D \sim 1/\rho$. If the inelastic time had a dependence $\tau_{in} \sim \rho/T$, however, the experimental results on Au-Pd could be understood. Though no inelastic mechanism has been identified which has this dependence, magnetoresistance studies of thick, 3D In-oxide films do show such a dependence of τ_{in} on ρ and T for that system.[30a]

Other experiments on 1D metal wires have been carried out by Chaudhari and co-workers at IBM[31] and by White and co-workers.[32] The IBM work used wires and films of W-Re, an amorphous superconductor. Electron beam contamination resist patterning was used. Experimental results agreed quantitatively with those for Au-Pd wires, once superconducting fluctuation effects were subtracted. Since W-Re is a superconductor with $T_c \sim 3.5$ K, measurements can also be made of the inelastic time just below T_c, using phase-slip resistance measurements. Results of such measurements[31b] are consistent with the inelastic times inferred from the localization measurements.[31a] However, subsequent theoretical work on localization effects above the transition temperature of a superconductor indicate that other mechanisms contribute to ΔR,[35] so that a more complex analysis of the data is required for extracting τ_{in}. We discuss this in the next section, in relation to experiments on Al films.

Experiments by White and co-workers on Cu, Ni, and Au-Pd wires used the procedure in Fig. 5f. Wires were produced on a thin membrane so that they could be inspected with TEM. A TEM picture of such a wire is shown in Fig. 6. In these studies it was found that low temperature resistance rise had to be carefully separated from a temperature dependent background due presumably to electron-phonon scattering. The resistance rise could be explained as being due to electron-electron interaction effects, given approximately as

$$\frac{\Delta R_{int}}{R} \sim \frac{L_{int}}{L_{36k\Omega}} \quad . \tag{5}$$

Furthermore, previous Au-Pd and W-Re results were shown to be consistent with the interaction mechanism, at least to within numerical factors of $\sim$2. If the interaction mechanism is to explain the full resistance rise, then the inelastic times must be even shorter than the very short values originally inferred.[30,31] Also, the unusual dependence on ρ seen in the Au-Pd results, Eq. 4, is not explained by the interaction mechanism. Since inelastic mechanisms in dirty 2D metal films were also not well understood at that time, it was clear that efforts needed to be directed towards understanding the inelastic scattering mechanism(s) itself.

Experiments on Aluminum: Films and Wires, and Other Recent Work

Recent experiments by Santhanam and Prober[33] have investigated the inelastic scattering rate in clean aluminum films and wires, specifically to understand inelastic mechanisms in a clean system where extensive transport studies have previously been done on single-crystal samples, and on superconducting properties of thin films. Al readily forms thin continuous films which adhere well to most substrates; it is also a superconductor ($T_c \sim 1.4$K for the films studied). To allow both 2D and 1D samples to be produced, a lift-off process was employed. For linewidths >1 μm, photolithography was employed. For linewidths <1 μm, x-ray lithography was used. Lines as narrow as 400 Å are readily produced with edge-defined masks.[34]

Magnetoresistance studies were carried out for a number of film strips of thicknesses 150 and 250 Å, and widths 0.6 to 40 μm. The 40 μm strips are in the 2D limit. Sheet resistances were 1-4 ohms/square, corresponding to a mean free path $\ell \sim 100$ Å. Theoretical predictions for the magnetoresistance of 2D superconducting films above T_c include the effects of superconducting fluctuations,[35] localization effects,[36] and electron-electron interaction effects.[26] For the field range used, only the first two contributions are significant.

The experimental data on the wide, 2D films can be fit with the 2D theoretical expressions[35,36] at all temperatures, using a temperature-dependent value of τ_{in} and a temperature-independent value of the spin-orbit time, τ_{so}. Inelastic scattering rates are found to fit the simple form:

$$\tau_{in}^{-1} = A_1 T + A_3 T^3, \tag{6}$$

where the coefficients A_1 and A_3 are determined for each sample. The A_1 term is due to electron-electron scattering in a dirty 2D system, and agrees with the theoretical value given by

$$A_1 = \frac{e^2 R_\square}{2\pi\hbar^2} k_B \ln (T_1/T) \tag{7}$$

with $R_\square$ the sheet resistance and $T_1 = 9 \times 10^5 (k_F \ell)^3$. The investigated films should indeed be in the dirty 2D limit for electron-electron scattering. The A_3 term is due to electron-phonon scattering in a 3D system. The films should indeed be in the 3D regime with respect to the phonon wavelength at the higher temperatures where the T^3 term is dominant. ($\lambda_{phonon} \sim 750$ Å/T for Al; λ is thus less than the film thickness above 5K.) The theoretical value[37] of

A_3 is 9 x 10^6 $sec^{-1}K^{-3}$; this value is obtained[37] by averaging over the Fermi surface. Experimental values of A_3 are ∿50% larger. Given the theoretical and experimental uncertainties, this can be considered to be good agreement. The theoretical value of A_3 at specific Fermi surface locations has been confirmed experimentally (with single crystals) to about the same accuracy.[37]

For narrower strips, a deviation from the 2D form of the magnetoresistance is seen, at temperatures which correspond roughly to the strip width W being less than $\ell_{in}(T)$. This appears to signal the 2D to 1D crossover, which is expected to occur when $\ell_{in} > W$.[26a] This crossover is a strong confirmation of the actual length scale in the localization theory. The values of ℓ_{in} are large - a few μm at 2K. This indicates that experiments probing localization at a size scale ℓ_{in} may be possible with such clean films.

Other experiments on magnetoresistance of Al films have also recently been completed.[38,39] These have all been on films with larger values of $R_\square$. The data in all these experiments appear to be consistent with those discussed above. However in the case of Refs. 38, the methods of data analysis omitted aspects of the theory which have proven to be important.[33,39] Studies of films of high-resistivity, granular Al have been conducted by Gordon and co-workers. They find that $\tau_{in}^{-1} = A_1T + A_4T^4$ for the films with $R_\square > 50\Omega$. The T^4 term is ascribed to electron-phonon scattering in a dirty, 3D system. The conclusions reached by Santhanam and Prober for clean films, Eq. 6, and also for the high resistance films[39] appear to be generally applicable. The other experiments on Al films treat only 2D systems, and further discussion of the results is somewhat outside the domain of this chapter. Additional discussion is given in Refs. 33 and 39.

One other study of microfabricated 1D metal wires has been conducted recently[40] to determine the dependence of the resistance rise, ΔR, on sample length. Au-Pd triangular wires were formed, and silver contact pads were patterned by evaporating over a thin fiber which defined the gap between contact pads, and thus the wire length. The length scale found is 0.2 μm at 1.5K. This is consistent with the value of ℓ_{in} inferred from measurements on long wires.[29] The specific functional dependence of ΔR/R on wire length remains to be explained, however.

A final example of 1D metal wires is given by work on wires formed by filling etched particle tracks in mica with Au.[41] Wires produced were as small as 80 Å, the smallest to be studied in any experiment. The resistance rise seen is consistent in magnitude with that seen in lithographically-produced low resistivity wires,[32] although the temperature dependence of ΔR is not exactly proportional to $T^{-1/2}$ as had been found in previous studies.

In conclusion, studies of 1D conduction in fine metal wires have been fairly successful in verifying predictions of the weak localization theory. For cleaner films of Al, the inelastic scattering rate can be understood quantitatively as a sum of two terms due to electron-electron and electron-phonon scattering. Inelastic scattering processes in very dirty metal films and wires ($\rho > 100$ $\mu\Omega$-cm) still remain to be understood.

Experiments on 1D MOSFETs

MOSFETs (Metal-Oxide-Semiconductor-Field-Effect Transistors) represent an ideal proving ground for studying 2D electron transport, and have been the primary system used for confirming 2D localization theory.[42] In addition, since the gate voltage can be varied, the number of carriers can be directly controlled, unlike the case of metals. This extra variable can be of considerable importance in emphasizing different mechanisms.

Fabrication approaches. Two dimensional MOSFETs are made with standard IC fabrication technology, typically on <100> silicon. To emphasize localization effects over interaction effects, high mobility devices are required. This demands stringent cleanliness in the fabrication process, particularly for avoidance of Na ion contamination. High energy fabrication processes, such as electron beam lithography, should also be avoided if possible, as they create charged scattering centers in the oxide, reducing the mobility. Optical photolithography does not induce such damage. The highest mobility Si devices have $\mu \sim 20{,}000$ $cm^2/V\text{-}sec$ at $\sim$4K.[43,44]

Magnetoresistance and Hall effect studies have been conducted on 2D MOSFETs by a number of research groups.[27f,42,43,45] There appears to be consensus that the existing theory of localization can describe these results, although the underlying scaling theory has been questioned by one group.[45b] Inelastic scattering rates can be described by[27f,43b]

$$\tau_i^{-1} = A_1 T + A_2 T^2 \qquad (8)$$

with the A_1 and A_2 terms due to electron-electron scattering in dirty and clean limits respectively, or more simply by $\tau_i^{-1} = A_1 T$.[42] There is a question raised regarding the magnitude of A_1, and results obtained by various groups may not be in full agreement.[27f,43b]

The fabrication of 1D MOSFETs presents some special challenges which do not arise for wide MOSFETs. The essential difficulty is in producing a narrow ($\sim$0.1 μm) gate electrode without significantly reducing the device mobility. Two main fabrication approaches have been developed. In one approach, developed by Wheeler and co-workers

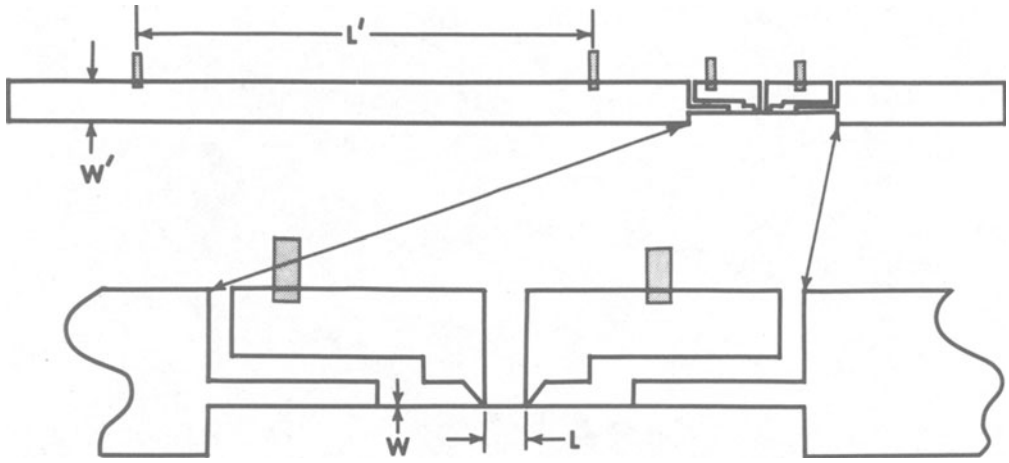

Fig. 8. Schematic representation of the gate structure of devices used in 1D MOSFET experiments at Yale. The darkened areas indicate locations of diffused-probe regions. Here W' = 100 μm, L' = 1050 μm and L = 25 μm. The data reported in Ref. 44 were from device AU310 where the mean value of W = 0.40 μm with a mean deviation of 0.02 μm.

at Yale,[44] optical projection lithography[6] is used to produce a photoresist mask for patterning a large area Al gate with wet chemical etching. With such techniques, the very high mobility achieved in the large area device is preserved. The geometry of the devices studied at Yale is shown in Fig. 8. Four-terminal measurement of resistance for both the wide and narrow sections is accomplished with doped or inversion-layer voltage probes. The oxide thickness is typically 350 Å, and the chip size is 2 mm. The minimum gate width produced is 3000 Å, with a rms width nonuniformity ≤5%.

The second major approach to 1D MOSFET fabrication has been developed at Bell Laboratories. Skocpol and co-workers[46] have produced MOSFETs as narrow as 400 Å using electron beam lithography to pattern, by lift-off, a Ni-Cr gate electrode. This gate then serves as an etch mask for reactive-ion etching of the 1000 Å SiO_2 layer and 2000 Å into the underlying silicon. The inversion layer thus

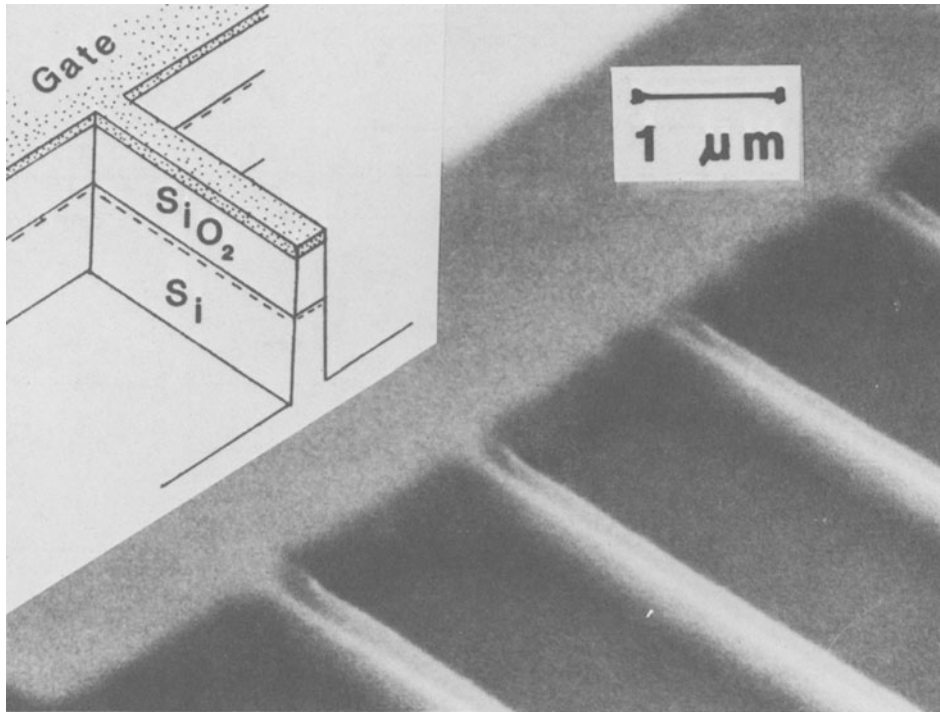

Fig. 9. Scanning electron micrograph of perspective view of several narrow MOSFET channels, and schematic diagram (inset) (From Ref. 46a)

sits in a pedestal, as shown in Fig. 9. Edge passivation is important, but fringing field effects, which can broaden the inversion layer relative to the geometrical gate width, should be negligible.

For these devices it is necessary to improve the mobility, which is significantly degraded by the lithographic processes. A 300°C thermal anneal is used after processing. The temperature limit is set by use of gold alignment marks. After annealing, mobilities up to 4000 cm^2/V-sec are obtained, with moderate threshold voltages. These devices are, in any case, the smallest MOSFETs produced to date. A 400 Å wide MOSFET is shown in Fig. 10.

Other approaches to the fabrication of 1D MOSFETs have been developed. The two approaches discussed above dealt with inversion layers. Fowler et al.[47] have produced very narrow accumulation layers in an FET structure where the accumulation layer is pinched down by the field of two p^+ regions on either side of the conducting strip. The spacing between p^+ regions is 1-2 μm, so that optical lithography can be used. Studies were carried out in the regime of

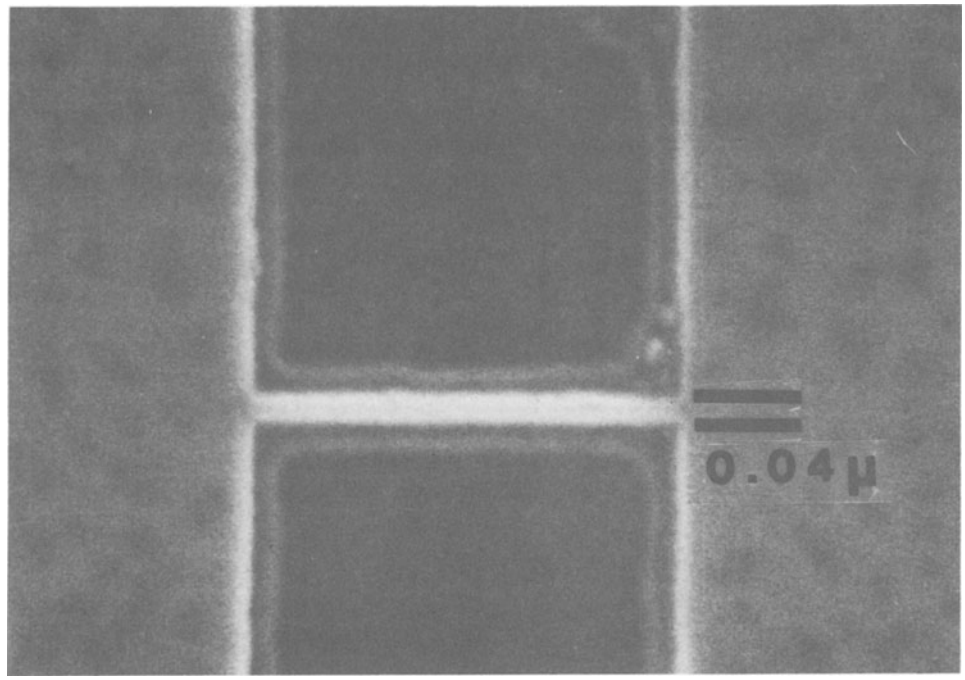

Fig. 10. SEM of narrow MOSFET; gate width is 400 Å, and gate length is 0.9 μm. (From Ref. 46b)

strong localization, where variable-range hopping is the main conduction mechanism. A transition from 2D to 1D hopping is observed as the channel width is reduced.

An edge-defined gate technique (Fig. 5f) has been developed by Kwasnick and co-workers.[48] Studies have been largely in the regime of strong localization. A topologically similar approach has been developed by Speidell[49] using the edge of a photoresist layer instead of an etched step.

Experimental Results: 1D Localization and Interaction Effects, and 1D Density-of-States. Low temperature studies of the temperature-dependent resistance and magnetoresistance have been carried out on the narrow inversion-layer devices.[44,46] Both sets of studies find that localization and interaction effects contribute in similar magnitude to the resistance rise, so that analysis of the temperature-dependent resistance does not allow a straightforward extraction of τ_{in}. Magnetoresistance measurements allow a more direct determin-

ation of localization effects (and thus τ_{in}), since, for the high mobility devices, the interaction effects depend only weakly on field at low fields.

Magnetoresistance measurements were carried out by Wheeler and co-workers on a number of 1D samples. The localization resistance in a finite magnetic field, H, is given by the expression[50,44]

$$\frac{\Delta R}{R} = \frac{R_{\square}}{2\pi\hbar/e^2}\frac{1}{W}\left(\frac{1}{D\tau_{in}} + \frac{W^2}{12\ell_H^4}\right)^{-1/2}. \tag{9a}$$

W is the channel width and ℓ_H is the magnetic length:[26] $\ell_H^2 = (\hbar c/2eH)$. The magnetoresistance, δR, is given as

$$\delta R = \Delta R(H) - \Delta R(H = 0). \tag{9b}$$

When $\ell_{in} > W$, Eq. 9a is accurate.

For the narrow samples at low temperatures (0.5K), it is found that

$$\tau_{in}^{-1}{}_{narrow} \sim T^{1/2}, \tag{10}$$

whereas for the wide (2D) samples, fits to the 2D magnetoresistance theory yield a rate

$$\tau_{in}^{-1}{}_{wide} \sim T . \tag{11}$$

These dependences are in accord with the theoretical predictions for electron-electron scattering in 1D and 2D dirty systems. The experimental magnitudes are also reasonably close to the theoretical predictions. Thus, the 1D experiments seem consistent with the theories for localization and for inelastic scattering in dirty systems.

In the course of these 1D experiments, it was noted that there was a curious variation of device resistance with the surface electron density, n_s, which is controlled by the gate voltage, V_g. Although no complete theory has been developed, there are indications[51] that such a variation of resistance with n_s may be due to quantization of the electron wavefunctions (and energy levels) by the narrow transverse width dimension of the gate, W. n_s is proportional to the Fermi energy E_F, and thus is proportional to $(V_g - V_{threshold})$. As n_s is increased, the higher quantum levels are filled. A very high density of states occurs when the Fermi level crosses an energy level. (Conduction along the <u>length</u> of the channel may also be

quantized, but with a much finer energy spacing, <<kT. Thus, only the width quantization should be significant.)

It is believed[51] that this particle-in-a-box width quantization affects the resistance through the localization resistance, ΔR, since ΔR depends on τ_{in} (Eqs. 1 and 3), and τ_{in} depends on the density of states at E_F.[44] Even though the elastic mean free path, $\ell \sim 1000$ Å, is less than the channel width, it is believed that the much longer inelastic length ℓ_{in} is the length over which the electron can sense quantizing boundaries. This is because over the distance ℓ_{in}, the electron has a constant energy. At the low temperatures where these effects are observed, ℓ_{in} is greater than the width.

The resistance variation as a function of V_g does show significant structure, with a typical spacing in gate voltage like that expected from the quantization arguments above. However, the structure is not very regular. This is due, at least in part, to width variations of the gate electrode, which cause the Fermi level to cross different quantized levels along the length of the channel.

To analyze quantitatively the lithographic requirements for width uniformity which will ensure that the Fermi level will be in a single quantum level, n, we list in Table IV the results of a calculation to determine the width difference ΔW to go from the n^{th} to the (n+1) level. As seen in the table, for current device widths (3000 Å) and current n_s values, a width variation of <100 Å must be achieved. This is a very demanding specification, but probably not impossible for narrower gates (500 Å) with currently available technology (See Figures 6 and 10, which indicate the type of lithographic uniformity now achieved.) Achieving such 100 Å-accuracy lithography is by no means trivial, especially if high device mobilities are required to allow smaller values of n_s. Producing these near-ideal 1D structures remains a significant future challenge.

Table IV. MOSFET Characteristics for 1D Density-of-States Studies

W (Gate Width)	n_s (cm^{-2})	E_F/k_B	n (Quantum Number at E_F)	$\Delta W_{n \to n+1}$
3000 Å	4×10^{12}	300 K	34	100 Å
500 Å	4×10^{12}	300 K	6	100 Å
500 Å	1×10^{12}	75 K	2	200 Å

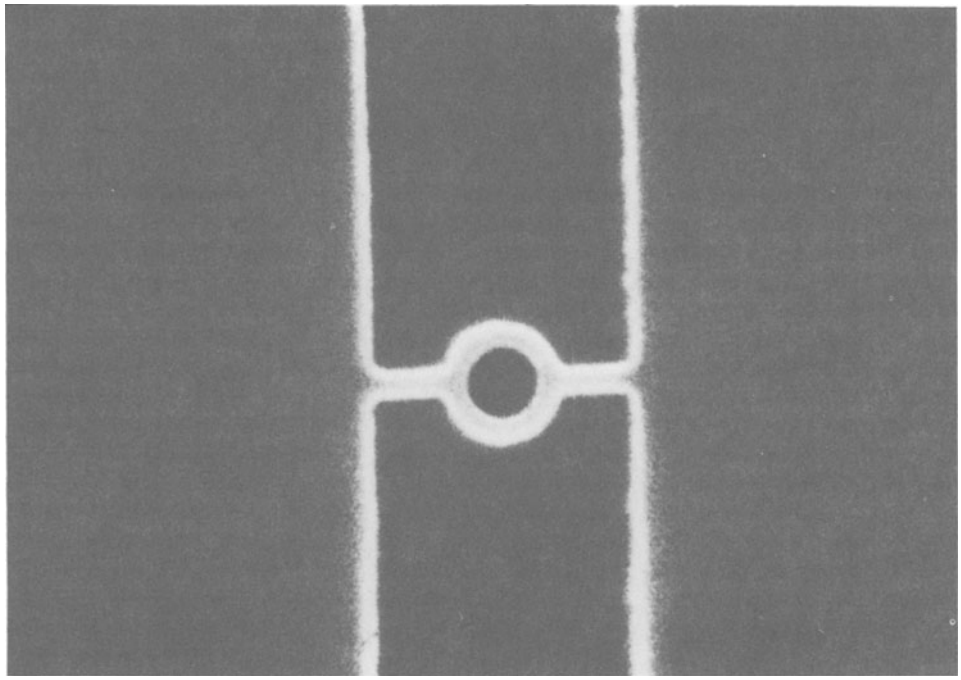

Fig. 11. SEM of 2000-Å diameter MOSFET ring, for study of normal-metal flux quantization. (From Ref. 46b)

Fluxoid Quantization in Nonsuperconducting Rings. A final issue which can be addressed with small MOSFET structures is the possibility of flux quantization in nonsuperconducting rings, first reported by Sharvin and Sharvin.[52] For such effects to be evident, the ring diameter should be less than $\sim \ell_{in}$, so that electron waves can typically remain in the same energy state and interact with each other around the ring.[26b] For metals, ℓ_{in} is usually short, and diameters <1 μm are required. For rings formed of an inversion layer, somewhat larger dimensions should be satisfactory. At Bell Laboratories, MOSFET rings as small as 2000 Å in diameter have been produced[46b]; an example is shown in Fig. 11. Experiments on these structures are at an initial stage.

The use of modulation-doped GaAs-AlGaAs heterostructures[53] can offer even larger values of ℓ_{in}: a value $\ell_{in} \sim 10$ μm at 1K has recently been observed in work at Bell Laboratories.[54] Preliminary experimental evidence appears to confirm the existence of fluxoid quantization in normal rings of these heterostructures, in structures of micron size.[54] Such a confirmation provides a striking demonstration of the power of microlithography when combined with ad-

vanced thin film deposition, for producing model systems for studies of low temperature electron quantum transport.

SCIENTIFIC STUDIES: SUPERCONDUCTING JOSEPHSON ARRAYS

Many experiments in recent years have studied properties of granular and composite metal films in order to probe issues of percolation, 2D superconducting transitions, and localization. Experimental studies of percolation and superconductivity in granular films are reviewed in this volume by Deutscher. When granular or composite films are used for studies of localization and 2D superconducting transitions, a question arises as to the effect of macroscopic nonuniformity and local inhomogeneities on the intrinsic behavior. There has been some progress in answering this question, at least for model types of macroscopic inhomogeneities.[55] Still, it is clearly of interest to study model systems, such as arrays, where macroscopic inhomogeneities can, at least in principle, be eliminated.

An ideal array to consider is that of superconducting islands which are coupled by Josephson tunneling to their nearest neighbors. The Josephson coupling energy is given as

$$E_J = \Phi_o I_o (1 - \cos\theta)/2\pi, \qquad (12)$$

where Φ_o is the flux quantum hc/2e, I_o is the critical current, and θ is the quantum mechanical phase difference across the Josephson junction. Such a discrete system, if large, is equivalent to the 2D X-Y model,[56] and can thus serve as a system in which the Kosterlitz-Thouless vortex unbinding transition can be studied.

Josephson junction arrays have been studied by Resnick and co-workers[57], Abraham and co-workers at Harvard[58], Berchier et al.[59] and by researchers at IBM.[60] The approach of the Harvard group is conceptually the simplest. In that work, superconducting (S) islands are coupled via Josephson tunneling thru a normal (N: non-superconducting) metal. This is a SNS tunneling structure. To form the array, a superconducting film of PbBi is first evaporated through a mechanical shadow mask consisting of a thin grid with a square array of holes as small as $\sim$10 μm. Without breaking vacuum, the mechanical mask is quickly moved away and a uniform Cu film is evaporated on top of the PbBi squares. This procedure is intended to avoid interface contamination,which can reduce Josephson coupling. It is also simple and inexpensive. Materials were selected to have minimal interdiffusion. The grid must be held in uniform contact with the substrate to avoid penumbral shadowing or scattering of the PbBi under the mask. Also, with the mask structure employed, Josephson coupling is not simply to nearest neighbors, though this is apparently a secondary

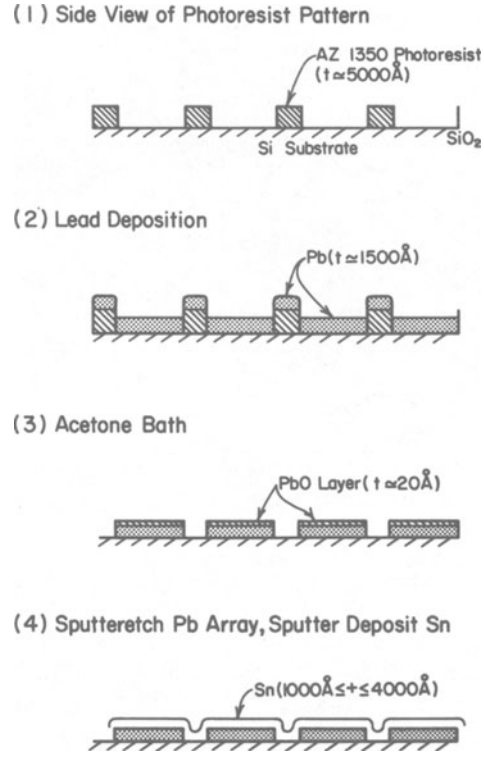

Fig. 12. Fabrication sequence for producing Pb-Sn-Pb proximity coupled Josephson arrays. (From work of Ref. 57)

issue. Vortex unbinding and periodic field response have been studied with these systems.

Patterning of SNS arrays with photolithography has been done by two groups.[57,59] In both cases, the normal metal was a second superconductor above its transition temperature. We shall describe the work of the Ohio State-Cincinnati group[57] as an example. This group formed a Pb-Sn-Pb tunnel junction array. Berchier and Sanchez have discussed the specifics of their fabrication procedure elsewhere.[59]

The procedure used to fabricate the Pb-Sn array is shown in Fig. 12. A Pb film is first evaporated onto a photoresist-patterned substrate, and a Pb dot pattern is produced by lift-off. Then, in a sputtering system, the substrate is Ar ion etched. Without breaking vacuum a Sn film is sputter deposited. The in-situ sputter cleaning is required to remove surface contamination. Ion beam sputter cleaning could serve the same purpose if the second film was to be deposited by evaporation. Such in-situ cleaning is necessary when an atomically clean surface or good metallurgical contact is required. The vortex unbinding transition was studied with the Pb-Sn arrays.

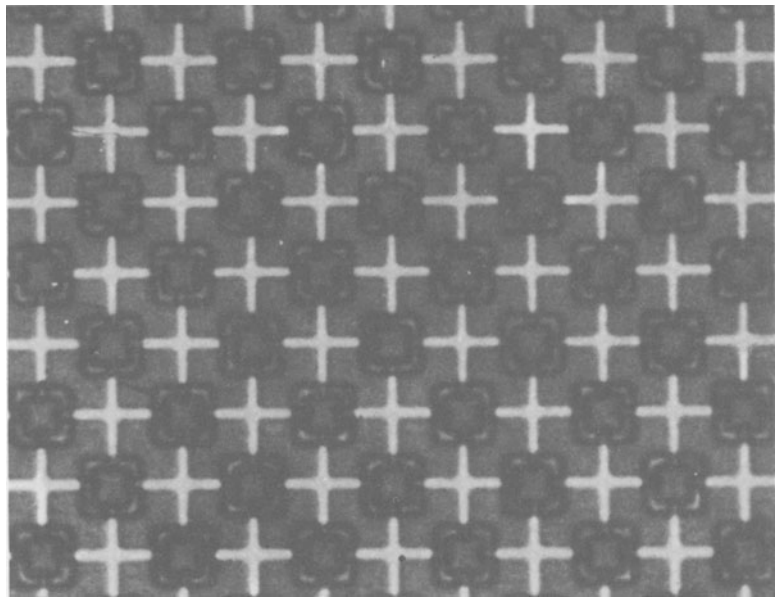

Fig. 13. Micrograph of a section of Pb-alloy Josephson junction array. Junction dimension is 2.5 μm. The total array consisted of 7200 junctions. (From Ref. 60a; see also Ref. 61.)

The last example of 2D Josephson junction arrays is work done at IBM. Standard processing was employed to form the oxide-barrier tunnel junctions.[61] Coupling was only to nearest neighbors for these arrays. An array of 7200 Pb-alloy junctions[60a] was used to study the effects of inhomogeneity when one fourth of the junctions were removed at random by laser "zapping" of the connections. A picture of a section of the uniform array is shown in Fig. 13. The tunnel junctions are located at the overlaps of the square rings and the crosses.

An array of 20,000 Nb-Nb tunnel junctions of 1-$(\mu m)^2$ area was used to study the vortex unbinding transition and the periodic modulation of the zero-bias resistance with magnetic field.[60b] For a similar array, critical currents of individual junctions varied by ±50%. It is not clear if the resulting variation in E_J (Eq. 12) is a problem, although experimental results were explainable in terms of behavior expected for a uniform array. The IBM Josephson process[61] can produce much more uniform Pb-alloy and Nb-Pb junctions for dimensions ≥2.5 μm.

Linear arrays of SNS microbridges have recently been produced at Stanford by deLozanne and co-workers using the step edge techniques described in a previous section.[22] The geometry of a single microbridge is shown in Fig. 14. The use of a step edge to define

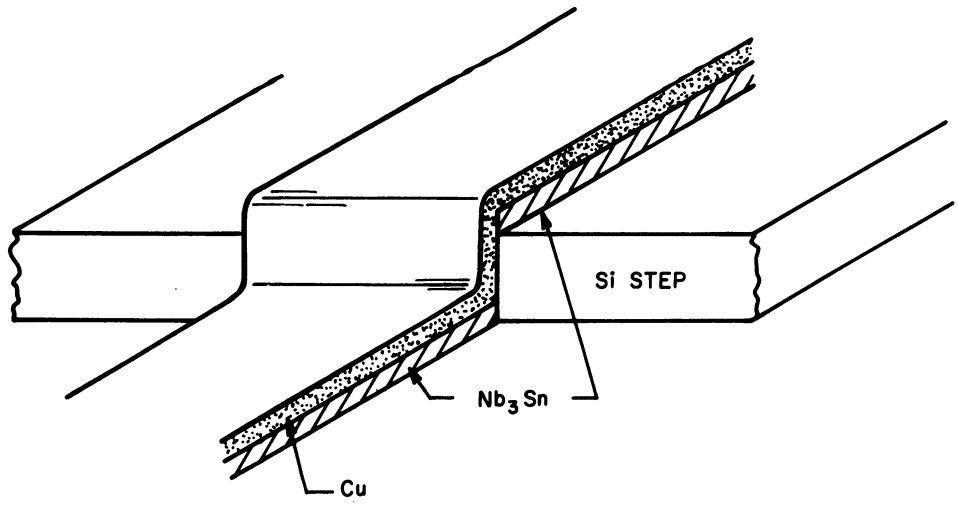

Fig. 14. Procedure for production of high-T_c SNS microbridge. Depositions of the normal metal (Cu or Au) and the superconductor (Nb_3Sn, Nb_3Ge) are from different angles. (From Ref. 22.)

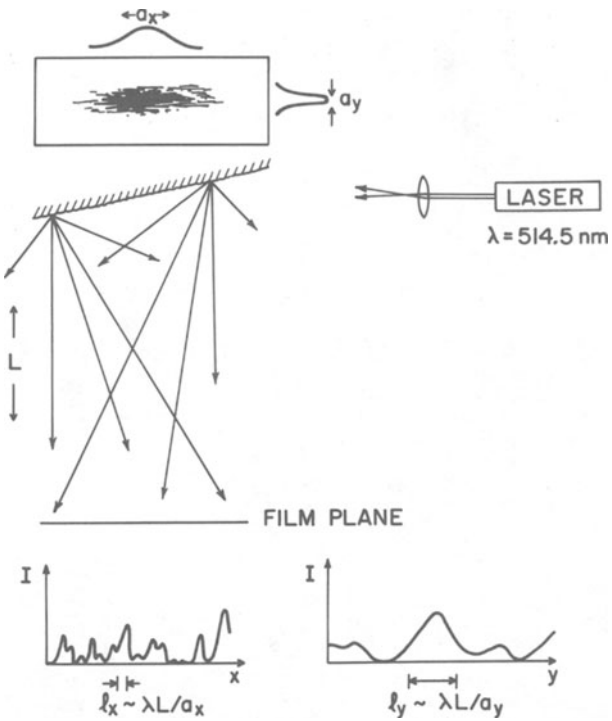

Fig. 15. Schematic of the optical system used to create the speckle patterns. The y direction is out of the plane of the figure. I is the exposure intensity at the film plane. This film is used as the exposure mask for photolithography.

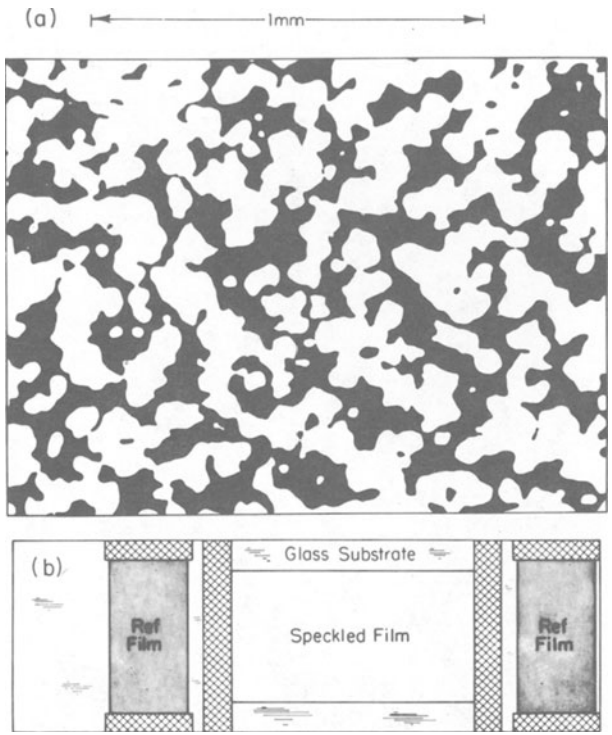

Fig. 16. (a) Photograph of a small section from an isotropic sample. The black areas are metal. (b) Sample geometry. The cross-hatched regions are the thick aluminum or NiCr contacts. (From Ref. 64.)

microbridge length leads to good uniformity of the critical currents for bridges in an array.

Other examples of array-like structures, though not of Josephson junctions, include Al films patterned with a triangular hole lattice[62] and films patterned by holographic resist exposure with a grating-like grid.[63] Both types of samples were used to study flux flow and pinning. Partially continuous films have been patterned by photoresist lift-off, where the exposure mask was produced by a laser speckle pattern, as shown in Figs. 15 and 16.[64] These partly continuous films were used in studies of percolation, in particular to test anisotropy effects. A final example is the construction of a metal dot pattern by angle evaporation onto an insulating substrate which had been etched with two crossed grating patterns. These samples were used to study surface-enhanced Raman scattering.[65]

Arrays have thus made effective contributions in a variety of scientific areas. One of the main difficulties in producing large arrays is production of the very complex masks required. Here again, the capabilities of modern integrated circuit facilities may be utilized. The large range of materials and fabrication approaches which can be employed should in the future allow many new scientific issues to be addressed.

CONCLUSIONS

In this chapter we have reviewed trends in modern microlithography. It is now possible to pattern on the 100 Å scale using either direct (electron beam) lithography or edge defined approaches. Etching and deposition now commonly employ directional ion processes, such as reactive ion etching and ion beam sputtering. These varied techniques provide a powerful set of microfabrication methods. These techniques have already led to real advances in our understanding of electron quantum transport in systems of reduced dimensionality, and the 2D vortex unbinding transition in superconductors. In the next five years, the ability to pattern at these unprecedented size scales will open up many new scientific challenges and opportunities.

Acknowledgements

Instructive discussions with numerous colleagues and collaborators are gratefully acknowledged. Particular thanks go to D. W. Face, R. E. Howard, Y. Imry, P. Santhanam, W. J. Skocpol, R. G. Wheeler and S. Wind for discussions relevant to this article. Research work at Yale University has been supported by the National Science Foundation and the Office of Naval Research.

REFERENCES

1. R. E. Howard and D. E. Prober, "Nanometer Scale Fabrication Techniques," in: VLSI Electronics: Microstructure Science, Vol. V, N. E. Einspruch, ed., Academic, New York (1982).
2. J. E. Lukens, AIP Conf. Proc. 44:198 (1978); R. E. Howard, P. F. Liao, W. J. Skocpol, L. D. Jackel, and H. G. Craighead, Science 221:117 (1983).
3. H. I. Smith, Proc. IEEE 62:1361 (1974).
4. A. N. Broers, IEEE Trans. Electron Devices ED-28:1268 (1981).
5. R. Newman (ed.), "Fine Line Lithography," North Holland Publ., Amsterdam (1980); I. Brodie and J. J. Muray, "Physics of Microfabrication," Plenum Press, New York (1982); also, Refs. 1-3, 6-12 in Ref. 1.
6. M. D. Feuer and D. E. Prober, IEEE Trans. Electron Devices ED-28: 1375 (1981); chromatic aberration of microscope lenses is discussed by M. J. Brady and A. Davidson, Rev. Sci. Instrum. 54: Oct. (1983), to be published.
7. P. Grabbe, E. L. Hu, and R. E. Howard, J. Vac. Sci. Technol. 21:33 (1982), and references therein.
8. J. M. Moran, Solid State Technol. 24(4):195 (1981); M. Hatzakis, Solid State Technol. 24(8):74 (1981); B. J. Lin, E. Bassous, V. W. Chao, and K. E. Petrillo, J. Vac. Sci. Technol. 19:1313 (1981).
9. L. D. Jackel, R.E. Howard, E. L. Hu, P. Grabbe, and D. M. Tennant, Appl. Phys. Lett. 39:268 (1981); D. M. Tennant, L. D. Jackel, R. E. Howard, E. L. Hu, P. Grabbe, R. J. Capik, and B. S. Schneider, J. Vac. Sci. Technol. 19:1304 (1981).
10. P. S. Burggraaf, Semicond. Intl. (6)55 June (1983); K. Bartlett, G. Hillis, M. Chen, R. Trutna and M. Watts, SPIE Proc. 394, no. 05 (1983).
11. H. G. Craighead, R. E. Howard, L. D. Jackel, and P. M. Mankiewich, Appl. Phys. Lett. 42:38 (1983).
12. P. Grabbe, Rev. Sci. Instrum. 51:992 (1980).
13. R. B. Laibowitz, this volume; also A. N. Broers, W. W. Molzen, J. J. Cuomo, and N. D. Wittels, Appl. Phys. Lett. 29:596 (1976) and W. W. Molzen, A. N. Broers, J. J. Cuomo, J. M. E. Harper, and R. B. Laibowitz, J. Vac. Sci. Technol. 16:269 (1979).
14. D. C. Flanders and A. E. White, J. Vac. Sci. Technol. 19:892 (1981); D. C. Flanders, J. Vac. Sci. Technol. 16:1615 (1979), and D. C. Flanders, Ph.D. Thesis, MIT (1978).
15. D. C. Flanders, Appl. Phys. Lett. 36:93 (1980).

16a. K. E. Bean, IEEE Trans. Electron Devices ED-25:1185 (1978).

16b. H. Kroger, L. N. Smith, and D. W. Jillie, Appl. Phys. Lett. 39:280 (1981).

17. H. W. Lehmann and R. Widmer, J. Vac. Sci. Technol. 15:319 (1978); L. M. Ephrath, IEEE Trans. Electron Devices ED-28: 1315 (1981).

18. D. W. Face, S. T. Ruggiero, and D. E. Prober, J. Vac. Sci. Technol. A1:326 (1983); S. T. Ruggiero, D. W. Face, and D. E. Prober, IEEE Trans. Magn. MAG-19:960 (1983); a general review of ion beam techniques for material processing is given by J. M. E. Harper, J. J. Cuomo, and H. R. Kaufman, Ann. Rev. Mat. Sci. 13:413 (1983).
19. M. Gurvitch, M. A. Washington, and H. A. Huggins, Appl. Phys. Lett. 42:472 (1983); S. T. Ruggiero, E. Track, and D. E. Prober, to be published. See also Ref. 16b.
20. D. E. Prober, M. D. Feuer, and N. Giordano, Appl. Phys. Lett. 37:94 (1980).
21. M. D. Feuer and D. E. Prober, Appl. Phys. Lett. 36:226 (1980).
22. A. de Lozanne, M . S. DiIorio, and M. R. Beasley, Appl. Phys. Lett. 42:541 (1983), and private communication
23. G. J. Dolan, Appl. Phys. Lett. 31:337 (1977); E. L. Hu, L. D. Jackel, and R. E. Howard, IEEE Trans. Electron Devices ED-28:1382 (1981).
24. L. D. Jackel, J. P. Gordon, E. L. Hu, R. E. Howard, L. A. Fetter, D. M. Tennant, R. W. Epworth, and J. Kurkijärvi, Phys. Rev. Lett. 47:697 (1981).
25. a. G. J. Dolan, T. G. Phillips, and D. P. Woody, Appl. Phys. Lett. 34:347 (1979) and b. A. D. Smith, R. A. Batchelor, W. R. McGrath, P. L. Richards, H. van Kempen, D. E. Prober, and P. Santhanam, Appl. Phys. Lett. 39:655 (1981).
26. a. Y. Imry, this volume, and J. Appl. Phys. 55:1812 (1981); b. H. Fukuyama, this volume, and Surf. Sci. 113:489 (1982).
27. a. A. Schmid, Z. Phys. 259:421 (1973); b. G. Bergmann, Z. Phys. B48:5 (1982); c. G. Giuliani and J. J. Quinn, Phys. Rev. B26:4421 (1982) - we identify $|p-p_F|$ with the thermal energy kT; d. E. Abrahams, P. W. Anderson, P. A. Lee, and T. V. Ramakrishnan, Phys. Rev. B24:6783 (1981); e. B. L. Altshuler, A. G. Arovov, D. E. Khmel'nitsky, J. Phys. C 15:7367 (1982); f. R. A. Davies and M. Pepper, J. Phys. C. 16:L353 (1983).
28. D. J. Thouless, Phys. Rev. Lett. 39:1167 (1977) and Solid State Commun. 34:683 (1980).
29. a. N. Giordano, W. Gilson, and D. E. Prober, Phys. Rev. Lett. 43:725 (1979); b. N. Giordano, Phys. Rev. B22:5635 (1980).
30. N. Giordano, in Physics in One Dimension, J. Bernasconi and T. Schneider, eds., Springer-Verlag, New York (1981), p.310, and Ref. 29b.
30a. Z. Ovadyahu, to be published.
31. P. Chaudhari and H.-U. Habermeier, Phys. Rev. Lett. 44:40 (1980), and Solid State Commun. 34:687 (1980); b. P. Chaudhari, A. N. Broers, C. C. Chi, R. Laibowitz, E. Spiller, and J. Viggiano, Phys. Rev. Lett. 45:930 (1980).
32. A. E. White, M. Tinkham, W. J. Skocpol, and D. C. Flanders, Phys. Rev. Lett. 48:1752 (1982).
33. P. Santhanam and D. E. Prober, to be published.

34. S. Wind, unpublished.
35. A. I. Larkin, Pis'ma Zh. Eksp. Teor. Fiz. 31:239 (1980), [JETP Lett. 31:219 (1980)].
36. S. Hikami, A. I. Larkin, and Y. Nagaoka, Prog. Theor. Phys. 63:707 (1980).
37. W. E. Lawrence and A. B. Meador, Phys. Rev. B18:1154 (1978).
38. a. Y. Bruynseraede, M. Gijs, C. Van Haesendonck, and G. Deutscher, Phys. Rev. Lett. 50:277 (1983); a recent reanalysis of this data yields the result of Eq. 6. b. M. E. Gershenson, V. N. Gubankov, and Yu. E. Zhuralev, Solid State Commun. 45:87 (1983).
39. J. M. Gordon, C. J. Lobb, and M. Tinkham, Phys. Rev. B, to be published.
40. J. T. Masden and N. Giordano, Phys. Rev. Lett. 49:819 (1982).
41. W. D. Williams and N. Giordano, Bull. Am. Phys. Soc. 28:486 (1983), and private communication.
42. R. C. Dynes, Physica 109-110B:1857 (1982); D. J. Bishop, R. C. Dynes and C. C. Tsuei, Phys. Rev. B26:773 (1982).
43a. R. G. Wheeler, Phys. Rev. B24:4645 (1981)b. K. K. Choi, Phys. Rev. B, to be published.
44. R. G. Wheeler, K. K. Choi, A. Goel, R. Wisnieff, and D. E. Prober, Phys. Rev. Lett. 49:1674 (1982).
45. a. Y. Kawaguchi and S. Kawaji, Surf. Sci. 113:505 (1982); b. R. A. Davies, M. Pepper, and M. Kaveh, J. Phys. C 16:L285 (1983).
46. a. W. J. Skocpol, L. D. Jackel, E. L. Hu, R. E. Howard, and L. A. Fetter, Phys. Rev. Lett. 49:951 (1982) and Physica 117-118B:667 (1983); b. L. D. Jackel, Bull. Am. Phys. Soc. 28:401 (1983); W. J. Skocpol, Bull. APS 28:276 (1983).
47. A. B. Fowler, A. Hartstein, and R. A. Webb, Phys. Rev. Lett. 48:196 (1982).
48. R. F. Kwasnick, M. A. Kastner, and J. Melngailis, Bull. Am. Phys. Soc. 28:322 (1983).
49. J. L. Speidell, J. Vac. Sci. Technol. 19:693 (1981).
50. B. L. Altshuler and A. G. Aronov, JETP Lett. 33:499 (1981).
51. R. G. Wheeler, Bull. Am. Phys. Soc. 28:276 (1983); also, D. E. Prober, Bull. Am. Phys. Soc. 28:401 (1983).
52. B.L. Al'tshuler, A. G. Aronov, B. Z. Spivak, D. Yu. Sharvin, and Yu. V. Sharvin, JETP Lett. 35:588 (1983).
53. R. Dingle, H. Störmer, A. Gossard and W. Wiegmann, Appl. Phys. Lett. 33:665 (1978).
54. G. E. Blonder and R. C. Dynes, private communication and to be published.
55. Y. Gefen, D. J. Thouless, and Y. Imry, Phys. Rev. B, to be published.
56. J. E. Mooij and P. Minnhagen, this volume; Y. Imry, AIP Conf. Proc. 58:141 (1980).
57. D. J. Resnick, J. C. Garland, J. T. Boyd, S. Shoemaker, and R. S. Newrock, Phys. Rev. Lett. 47:1542 (1981).

58. D. W. Abraham, C. J. Lobb, M. Tinkham, and T. M. Klapwijk, Phys. Rev. B26:5268 (1982).
59. J. L. Berchier and D. Sanchez, Rev. de Physique Appl. 14: 757 (1979), and references therein.
60. a. A. Davidson and C. C. Tsuei, Physica 108B:1243 (1981); b. R. F. Voss and R. A. Webb, Phys. Rev. B25:3446 (1982).
61. J. H. Greiner et al., IBM J. Res. Dev. 24:195 (1980); R. F. Broom et al., IEEE Trans. Electron Dev. ED-27:1998 (1980).
62. A. T. Fiory, A. F. Hebard and S. Somekh, Appl. Phys. Lett. 32:73 (1978).
63. O. Daldini, P. Martinoli, J. L. Olsen, and G. Berner, Phys. Rev. Lett. 32:218 (1974).
64. L. N. Smith and C. J. Lobb, Phys. Rev. B20:3653 (1979).
65. P. F. Liao, J. G. Bergman, D. S. Chemla, A. Wokaun, J. Melngailis, A. M. Hawryluk, and N. P. Economou, Chem. Phys. Lett. 82:355 (1981).